atmosphere

MDPI

Article

Screening of Absorbents for Viscose Fiber CS_2 Waste Air and Absorption–Desorption Process

Ruixue Xiao, Kefan Chao, Ju Liu, Muhua Chen, Xinbao Zhu and Bo Fu *

Jiangsu Co-Innovation Center of Efficient Processing and Utilization of Forest Resources, College of Chemical Engineering, Nanjing Forestry University, Nanjing 210037, China
* Correspondence: fubo@njfu.edu.cn

Abstract: Screening of absorbents is essential for improving the removal rate of carbon disulfide (CS_2) waste air by absorption. In this work, the UNIFAC model in Aspen Plus was utilized to calculate the excess Gibbs function and absorption potential of the binary system of CS_2 with various alcohols, ethers, esters, amines, and aromatic hydrocarbons. The results were used to quantitatively compare the efficiency of each solvent for CS_2 absorption. The theoretical predictions were then verified by absorption experiments in a packed tower. The results showed that the performance of various solvents to CS_2 roughly followed the order of esters < alcohols < amines < heavy aromatics < glycol ethers. Meanwhile, N-methyl-2-pyrrolidone (NMP) is the optimal absorbent for CS_2 waste air treatment. Additionally, the process parameters of absorption and desorption of NMP were optimized. The results illustrated that the average mass removal efficiency of CS_2 by NMP is 95.2% under following conditions: liquid–gas ratio of 3.75 $L \cdot m^{-3}$, a temperature of 20 °C, and inlet concentration lower than 10,000 $mg \cdot m^{-3}$. Under the conditions of 115 °C, 10 kPa, and a desorption time of 45 min, the average desorption rate of CS_2 is 99.6%, and the average water content after desorption is 0.39%. Furthermore, the recycled lean liquid can maintain an excellent CS_2 purification effect during the recycling process.

Keywords: CS_2 waste air; Aspen Plus; excess Gibbs function; absorption potential; process optimization

Citation: Xiao, R.; Chao, K.; Liu, J.; Chen, M.; Zhu, X.; Fu, B. Screening of Absorbents for Viscose Fiber CS_2 Waste Air and Absorption–Desorption Process. *Atmosphere* **2023**, *14*, 602. https://doi.org/10.3390/atmos14030602

Academic Editors: Cinzia Perrino and Kumar Vikrant

Received: 8 February 2023
Revised: 10 March 2023
Accepted: 20 March 2023
Published: 22 March 2023

1. Introduction

Viscose fiber is classified as regenerated cellulose prepared using natural cellulose as raw material through the viscose process. With the merits of absorbing features and excellent performance, viscose fiber has been widely used. As the most critical solvent, carbon disulfide (CS_2) is often used to produce viscose fiber. Because of this, CS_2 is inevitably emitted into the atmosphere through exhaust gases [1,2]. Meanwhile, studies on the traceability of CS_2 in the atmosphere have also confirmed that human activity is the primary source of CS_2 [3–5]. Atmospheric CS_2 is rapidly oxidized to carbonyl sulfide and sulfur dioxide, which play an essential role in the global sulfur cycle [6]. The newly produced carbonyl sulfide and CS_2 affect stratospheric ozone levels and contribute to acid rain formation [4]. Furthermore, CS_2 is a dual odorous and harmful gas [7], which not only damages the human reproductive system [8], but also causes hearing loss [9,10]. Moreover, Schramm et al. [11] reported that long-term exposure to CS_2 increases the risk of cardiovascular disease in humans. Therefore, it is urgent to achieve efficient recovery and environmental treatment of CS_2 waste air in industrial processes.

Currently, the treatment technology of CS_2 waste air can be divided into two categories: elimination and recovery [2]. The elimination technologies mainly include catalytic hydrolysis [12–15], oxidation [16,17], and biodegradation [18–20]. Elimination technologies, as a promising strategy for CS_2 treatment, have attracted widespread scientific attention. However, the complex process and the issue of destroying the molecular structures of CS_2 considerably hamper its practical application in industrial processes, while the recovery

technologies mainly include adsorption [21–25] and absorption. The adsorption method performs excellent removal, which is particularly applied for CS_2 waste air with large air volumes and low concentrations [26–28]. However, the adsorption method has poor applicability due to the adsorbent being easily deactivated and hardly regenerated under the conditions of actual CS_2 waste air in viscose fiber plants. In contrast, the absorption method comes to the fore in the CS_2 waste air recovery strategy on account of the advantages of a simple process, convenient operation, recyclable absorbent, and suitability for treating high-concentration waste air. Thus, it has received the attention of many scholars. For instance, Heldebrant et al. [29] studied the absorption and desorption of CS_2 in three ionic liquids, drawing on the experience of CO_2 absorption. They noted that CS_2 reacts similarly to CO_2 towards amidine/alcohol and guanidine/alcohol blends. Huo et al. [30] developed the UDS-F solvent to decline the simulated CS_2 waste air concentration from 400 $mg \cdot m^{-3}$ to 79 $mg \cdot m^{-3}$ (atmospheric pressure, 50 °C, and the liquid–gas ratio of 500). Although the mass removal efficiency of UDS-F solvent obtained from their experiments was only 80.3% for CS_2 exhaust, its removal effect was already significantly better than that of the conventional absorbent N-methyldiethanolamine (MDEA).

It is well-known that the screening of absorbents is critical to enhance the mass removal efficiency and reduce process energy consumption and cost. Previously, some scholars have proposed methods for screening absorbents or evaluating absorbents' merits and demerits [31,32]. An absorbent screening method was established by Wang et al. [33] with SO_2 absorption capacity and desorption reaction heat values as indicators. Yet their method is inappropriate for the screening of absorbents for physical absorption processes. In addition, Lhuissier et al. [34] established a mass transfer model (i.e., SSR model) for predicting the total transfer coefficient of a packed tower. They successfully predicted the removal rate of VOCs, such as ethyl acetate, isopropanol, and toluene, from transformer oil and lubricant oil with the help of the SSR model. Rodriguez Castillo et al. [35] derived Henry's law constants between different ionic liquids and toluene or dichloromethane by measuring the liquid–gas partition coefficients at equilibrium and then measured the diffusion coefficients of the gas molecules in the ionic liquid using a thermogravimetric microbalance (IGA-003). Finally, they used the above physical parameters obtained from these experiments to simulate the absorption process and evaluate the removal of toluene and methylene chloride from 23 different ionic liquids. Wang et al. [36] used IGA-003 to evaluate the absorption effect of dichloromethane in [Bmim][PF6] through a similar research approach. The difference is that they obtained data on the solubility of dichloromethane in [Bmim][PF6] at different pressures and then used a thermodynamic model fit to obtain Henry's law constant. Although the scholars mentioned above provided three different methods for screening or evaluating absorbents, each requires extensive experiments to provide mass transfer data. This experimental process is costly and time-consuming; for example, each set of solubility data in the study of Wang et al. [36] took over 72 h. Meanwhile, IGA-003 requires a very low saturation vapor pressure of the solvent being measured, which limits its use in assessing the physical property data between organic solvents and exhaust gases. Furthermore, to our knowledge, no scholars have proposed a simple sorbent screening method in which CS_2 was selected as the primary treatment target.

In this paper, the CS_2 absorbers were effectively screened based on the theory of excess Gibbs function and absorption potential. Then, the feasibility of this theoretical prediction method was verified through the absorption experiment. Moreover, the absorption and desorption process parameters were experimentally optimized, laying the foundation for further industrial applications. The study results provide specific theoretical support for the resource recovery of CS_2 waste air from viscose fiber plants and also provide an academic reference for the design of absorber compound formulations.

2. Materials and Methods

2.1. Experimental Reagents

Table 1 presents the reagents utilized in the experiments along with their respective specification parameters.

Table 1. Reagent specifications.

Experiment Reagent	Purity
N-Methyl-2-pyrrolidone (NMP)	99.7%
Ethylene glycol butyl ether acetate (BGA)	99.7%
Ethylene glycol (EG)	99.7%
N,N-Dimethylformamide (DMF)	99.7%
Ethylene glycol monobutyl ether (2-Butoxyethanol, BE)	99.7%
1,2,4-Trimethylbenzene (TMB)	99.5%
Ethanol absolute	99.7%
Triethanolamine (TEA)	99.7%
Diethylamine (DEA)	99.7%
Copper acetate	99.7%
Karl Fischer reagent	99.7%
CS_2	99.5%

Note: The manufacturing company is Sinopharm Chemical Reagent Co., Ltd. (Shanghai, China).

2.2. UNIFAC Model Simulation Calculation

The excess Gibbs function (G^E) of the binary system is expressed as Equation (1).

$$\begin{gathered} G^E = RT\left(n_1 \ln \frac{\xi_{11}}{x_1} + n_2 \ln \frac{\xi_{22}}{x_2}\right) \\ \xi_{11} = \frac{x_{11}V_{m1}}{x_{11}V_{m1}+x_{21}V_{m2}};\ \xi_{22} = \frac{x_{22}V_{m2}}{x_{12}V_{m1}+x_{22}V_{m2}} \end{gathered} \tag{1}$$

where x_i is i-molecular macromolecular fraction, ξ_{11} and ξ_{22} are local volume fractions, x_{ij} is the local molecular fraction of j-molecules around i-molecules, and V_{m1} and V_{m2} both represent the local molecular volume.

If $V_{m1} \approx V_{m2}$, $\xi_{11} \approx x_{11}$, $\xi_{22} \approx x_{22}$ can be obtained according to Equation (1). When the attraction between different molecules is stronger than that between the same molecules, then $\xi_{11} < x_1, \xi_{22} < x_2$. The further conclusion is that $G^E < 0$, and the smaller G^E illustrates the stronger attraction between dissimilar molecules. The maximum excess Gibbs function $(G^E_{\max})$ is an extreme point of G^E that exists under a certain temperature and pressure. The value of $G^E_{\max}$ is inversely proportional to the affinity between the absorbent molecules.

The absorption potential (ψ_i) of the binary system is calculated by Equation (2).

$$\psi_i = \frac{1}{\gamma_i^\infty} \tag{2}$$

where ψ_i is the absorption potential, and γ_i^∞ is the infinite dilution activity coefficient of the i-component in the binary system. ψ_i can reflect the solubility of a component in a solvent within a certain range; a larger value of ψ_i shows a better compatibility of the corresponding solute with the solvent.

$G^E_{\max}$ and ψ_i can be further calculated from the liquid–gas equilibrium data in the full concentration range of the binary system calculated by the UNIFAC model in Aspen Plus V11. Herein, $G^E_{\max}$ and ψ_i of the binary system composed of CS_2 and 30 pure solvents (water, alcohols, glycol ethers, esters, amines, aromatic hydrocarbons, etc.) were calculated, respectively. In order to verify the feasibility of extending the absorbent screening theories of $G^E_{\max}$ and ψ_i into the screening of CS_2 waste air absorbents, we selected the solvents from the abovementioned solvents for absorption experiments.

2.3. Experimental Method

2.3.1. Absorption Experiment Process

The specified concentration of CS_2 waste air was simulated by bubbling. The CS_2 waste air flows from bottom to top in the tower, and the absorbent contacts the gas countercurrent in the tower. After the absorption treatment, the tail gas enters the condensation system, and the absorption-rich liquid is extracted from the discharge port of the lower section of the absorption tower.

2.3.2. Experimental Analysis

The concentration of CS_2 gas was measured by DEA spectrophotometry (GB/T 14680-93) [37,38]. The specific measurement method is as follows:

(1) Preparation of absorption solution: 0.0500 g of copper acetate was dissolved in anhydrous ethanol in a 100.0 mL volumetric flask, and the volume was fixed and stored in a refrigerator at low temperature. After adding 300.0 mL of absolute ethanol to the 500.0 mL volumetric flask, 10.0 mL of copper acetate ethanol solution, 2.5 mL of DEA, and 2.5 mL of triethanolamine were added to the solution in sequence. After the above operations, anhydrous ethanol was used to make up the volume to the mark to obtain the absorption solution. (The above solutions need to be used and prepared now.)

(2) Preparation of CS_2 standard solution: 15.0 mL of absolute ethanol and 1 to 2 drops of CS_2 were sequentially added to a 25.0 mL volumetric flask, and the mass was recorded (accurate to 0.0001 g) with the stopper closed. Absolute ethanol was used to bring up to the mark and calculate the concentration of CS_2. The above solution was then diluted with absolute ethanol to contain about 10.00 μg of CS_2 standard solution per milliliter.

Draw the CS_2 standard curve: The standard solutions in Table 2 were prepared in 10 colorimetric tubes (10.0 mL) with stoppers. After each tube was mixed evenly, it was placed for 20 min. The absorbance of different samples was measured with absolute ethanol as a reference (435 nm, 3 cm cuvette). The CS_2 standard curve was plotted as shown in Figure 1.

Table 2. CS_2 content corresponding to different standard solutions.

No.	0	1	2	3	4	5	6	7	8	9	10
Absorbent (mL)	10.0	9.9	9.8	9.7	9.6	9.5	9.4	9.3	9.2	9.1	9.0
Standard solution (mL)	0	0.1	0.2	0.3	0.4	0.5	0.6	0.7	0.8	0.9	1.0
CS_2 content (μg)	0	3.92	7.84	11.76	15.68	19.60	23.52	27.44	31.36	35.28	39.20

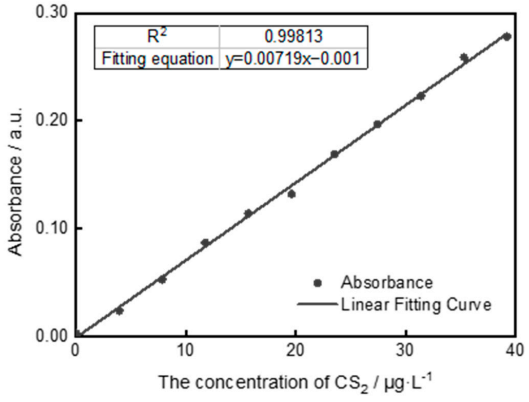

Figure 1. CS_2 standard curve.

2.3.3. CS_2 Gas Mass Concentration

Gas sampling was carried out using an absorbing liquid in an ice-water bath, the sample was placed at room temperature, and the sample liquid was prepared. Take an appropriate amount of sample into a 10.0 mL colorimetric tube with a stopper, add absorbing solution to the mark, and shake well. Then, follow the steps of drawing a standard curve, and check the content of CS_2 on the standard curve.

The formula for calculating the mass concentration of CS_2 gas is shown in Equation (3).

$$C = \frac{mV_1}{V_2V_n} \tag{3}$$

where C is the concentration of CS_2 in the measured gas, mg·m^{-3}; m is the amount of CS_2 in the sample liquid taken during the sample measurement, μg; V_1 is the constant volume of the sample solution, mL; V_2 is the volume of the sample solution taken during the measurement, mL; and V_n is the gas production volume in the standard state, L.

2.3.4. Mass Removal Efficiency for CS_2

The calculation formula of the CS_2 mass removal efficiency is shown in Equation (4) [34].

$$\eta_1 = \frac{C_{in} - C_{out}}{C_{in}} \times 100\% \tag{4}$$

where η_1 is the mass removal efficiency for CS_2; C_{in} is the intake concentration for CS_2, mg·m^{-3}; and C_{out} is the CS_2 waste air concentration, mg·m^{-3}.

2.4. Absorption and Desorption Process

2.4.1. Absorption Process

The absorption experiment device shown in Figure 2 is used in the study of the absorption process. The influence of process parameters such as liquid–gas ratio, absorbent temperature, and intake air concentration on the mass removal efficiency, is considered, and the optimal absorption process conditions are determined through multiple sets of experiments.

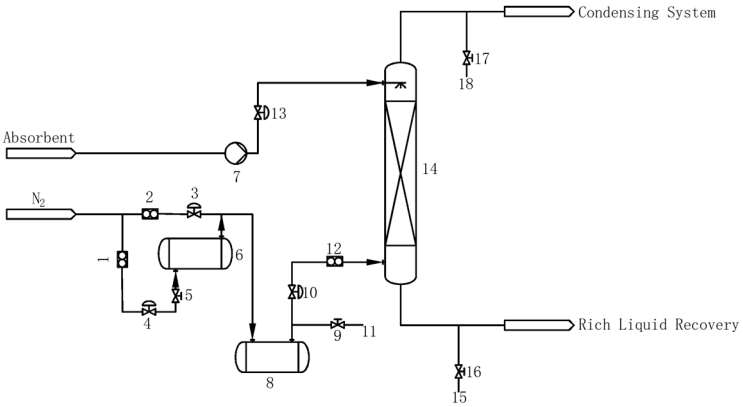

Figure 2. Absorption experiment setup: 1, 2, 12—rotameter; 3, 4, 10, 13—valve; 5, 9, 16, 17—stop valve; 6—CS_2 storage tank; 7—peristaltic pump; 8—mixing tank; 11, 15, 18—sampling test point; 14—absorption tower.

1. The effect of the liquid–gas ratio on mass removal efficiency

Under the condition that other factors remain unchanged, the liquid–gas ratio is adjusted by fixing the gas flow rate and adjusting the liquid flow rate. The other relevant experimental conditions are as follows: the intake air concentration is 8000 mg·m^{-3}, the gas flow rate is 0.24 m^3·h^{-1}, and the absorption temperature is 20 °C.

2. The effect of temperature on the mass removal efficiency

When investigating the effect of different temperatures on the mass removal efficiency of CS_2, the remaining relevant experimental conditions are: the intake air concentration is 8000 mg·m^{-3} and the liquid–gas ratio is 3.75 L·m^{-3}.

3. The effect of intake air concentration on the mass removal efficiency

When investigating the effect of different intake air concentrations on the CS_2 mass removal efficiency, the remaining relevant experimental conditions are: temperature 20 °C, liquid–gas ratio 3.75 L·m^{-3}.

2.4.2. Factors Affecting the Resorption Performance of Regeneration Lean Liquid

Generally speaking, the water content and CS_2 content in the absorbent are the main factors affecting the absorption performance of the regeneration lean liquid. Using the absorption apparatus depicted in Figure 2, this study investigated the influence of water and CS_2 contents on the mass removal efficiency of the regenerated lean liquid. Considering that the water and CS_2 contents in the absorbent have a synergistic effect on the mass removal efficiency, 0.5‰ of CS_2 was added to the absorbent with different water contents to investigate the synergistic effect on the mass removal efficiency (the intake air concentration was 8000 mg·m^{-3}; the liquid–gas ratio was 3.75 L·m^{-3}; the temperature was 20 °C).

The moisture content was measured using a Karl Fischer method trace moisture analyzer (BYES-8, Bangyi Precision Measuring Instrument Co., Ltd., Shanghai, China), and the formula for calculating the moisture content is (Equation (5)):

$$W = \frac{T \times V}{m} \times 100\% \quad (5)$$

where W is the moisture content, %; T is the titer of Karl Fischer reagent in water, g/mL; V is the injection volume, mL; and m is the quality of the sample, g.

The content of CS_2 in the liquid before and after desorption was measured by UV spectrophotometer. The calculation formula of CS_2 desorption rate is (Equation (6)):

$$\eta_2 = \frac{m_1 - m_2}{m_1} \times 100\% \quad (6)$$

where η_2 is the CS_2 desorption rate, %; m_1 is the CS_2 content in the rich liquid before desorption, g; and m_2 is the residual CS_2 content in the lean liquid after desorption, g.

2.4.3. Desorption Process

The main factors that influence the desorption effect are temperature, pressure, and time. To simulate the absorption of rich liquid, 1% water and 1.5‰ CS_2 are added to the absorbent. The effect of temperature on the analytical effect is analyzed (10 kPa, 20 min). The effect of pressure on the analytical effect is analyzed (115 °C, 20 min). The effect of time on the analytical effect is analyzed (115 °C, 15 kPa).

3. Results and Discussion

3.1. Analysis of Absorbent Screening Results

$G^E_{\max}$ and ψ_i of various solvent and CS_2 composition systems calculated by Aspen Plus V11 are shown in Table 3. As can be seen from Table 3, the absorption capability follows the order of esters < alcohols < amines < heavy aromatics < glycol ethers. Generally, according to the principle of "similarity-solubility", the order of the above should be glycol ethers > heavy aromatics > esters > alcohols > amines. However, CS_2 is a nonpolar reagent with a linear geometry similar to CO_2. It interacts with polar molecules via van der Waals forces and dipole–dipole interactions, which may be responsible for the superior affinity of CS_2 even in partially polar solvents. In fact, reports of the increased physical uptake of CO_2 resulting from van der Waals and dipole–dipole forces are commonplace [39,40].

Table 3. CS_2-solvent system maximum excess Gibbs function and absorption potential (20 °C, atmospheric pressure).

No.	Solvent	Molecular Formula	γ_i^∞	ψ_i	G_{max}^E/J·mol^{-1}
1	Water	H_2O	3979.458	2.513×10^{-4}	3157.89
2	EG	$C_2H_6O_2$	1.092	0.916	59.37
3	1-Pentanol	$C_5H_{12}O$	2.470	0.405	764.03
4	1-Octanol	$C_8H_{18}O$	1.530	0.654	428.75
5	Tripropylene glycol	$C_6H_{14}O_4$	1.876	0.533	788.37
6	Hexylene glycol	$C_6H_{14}O_2$	3.276	0.305	1175.25
7	Dibutyl ether	$C_8H_{18}O$	1.021	0.980	28.21
8	BE	$C_6H_{14}O_2$	0.511	1.959	−518.43
9	Diethylene glycol butyl ether	$C_8H_{18}O_3$	0.548	1.824	−514.26
10	Triethylene glycol monobutyl ether	$C_{10}H_{22}O_4$	1.205	0.830	301.70
11	Triethylene glycol dimethyl ether	$C_8H_{18}O_4$	1.259	0.794	283.23
12	Ethylene glycol monomethyl ether	$C_3H_8O_2$	0.769	1.300	−180.79
13	Ethylene glycol propyl ether	$C_5H_{12}O_2$	0.568	1.762	−423.45
14	Ethylene glycol monoethyl ether	$C_4H_{10}O_2$	0.648	1.544	−312.85
15	Propylene glycol monoethyl ether	$C_5H_{12}O_2$	2.420	0.413	784.49
16	Hexyl acetate	$C_8H_{16}O_2$	1.341	0.746	305.36
17	Propylene carbonate	$C_4H_6O_3$	4.467	0.224	1110.05
18	Ethylene glycol diacetate	$C_6H_{10}O_4$	3.017	0.331	1071.45
19	BGA	$C_8H_{16}O_3$	1.403	0.713	370.59
20	Ethylene glycol monoethyl ether acetate	$C_6H_{12}O_3$	1.904	0.525	602.54
21	Ethyl acetoacetate	$C_6H_{10}O_3$	2.952	0.339	995.69
22	Methyl salicylate	$C_8H_8O_3$	3.386	0.295	1167.32
23	DMF	C_3H_7NO	0.971	1.030	−18.01
24	MDEA	$C_5H_{13}NO_2$	3.821	0.262	852.26
25	Diisopropanolamine	$C_6H_{15}NO_2$	2.272	0.440	945.29
26	Diethanolamine	$C_4H_{11}NO_2$	1.902	0.526	645.66
27	TEA	$C_6H_{15}NO_3$	4.263	0.235	1636.44
28	NMP	C_5H_9NO	0.838	1.194	−132.00
29	Morpholine	C_4H_9NO	0.890	1.123	−83.30
30	TMB	C_9H_{12}	0.892	1.121	−64.61

The average mass removal efficiency results obtained after multiple groups of absorption experiments for NMP, BE, BGA, TMB, DMF, and EG are shown in Figure 3. The order of the mass removal efficiency of each solvent on CS_2 waste air is as follows: NMP > TMB > DMF > BE > BGA > EG. Combining with the data in Table 3, it can be seen that in addition to BE and EG, the mass removal efficiencies of NMP, TMB, DMF, and BGA on CS_2 waste air are consistent with the trends predicted by G_{max}^E and ψ_i. Combining the viscosity data of the six absorbents given in Table 4, it can be found that compared with NMP, TMB, and DMF, BE has good affinity, but its viscosity is large. Similarly, the viscosity of EG is greater than that of BGA. Overall, the greater viscosity leads to greater interfacial mass transfer resistance between the liquid–gas two phases, which in turn leads to a decrease in mass transfer rate and a poorer absorption effect [41]. Therefore, the mass removal efficiency of BE and EG on CS_2 waste air has an opposite trend to the predicted effect of G_{max}^E and ψ_i.

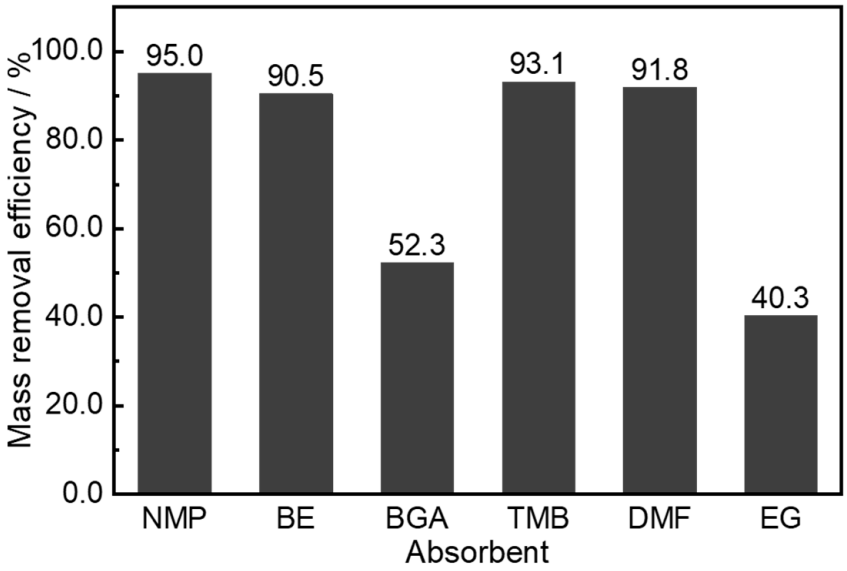

Figure 3. Average mass removal efficiency of CS_2 waste air by six different absorbents.

Table 4. Physical properties of absorbent.

Absorbent	Viscosity/mPa·s	Saturated Vapor Pressure/Pa	ORL-RAT LD_{50}/mg·kg^{-1}
NMP	2.08	31.5	3915
BE	3.35	77.5	1480
TMB	0.96	206.5	5000
DMF	0.87	394.3	2800
BGA	1.80	80.9	2400
EG	21.05	7.3	4700

Remark: The temperature is 20 °C; the pressure is atmospheric pressure; the LD50 test method is oral administration by rodents.

In conclusion, in the low viscosity system, it is feasible to use G^E_{max} and ψ_i to screen CS_2 absorbents, and it can greatly reduce the complicated screening process and expensive screening costs in previous studies. At the same time, it can be seen that NMP is a CS_2 waste air absorbent with good compatibility with CS_2 waste air, low volatility, and slight toxicity.

3.2. NMP Solution Absorption Process Conditions

The NMP absorption process study using experiments is shown in Figure 4. It can be seen from Figure 4a that when the liquid–gas ratio does not reach 3.75 L·m^{-3}, the CS_2 mass removal efficiency increases significantly, and the change tends to be gentle after reaching 3.75 L·m^{-3}. The improvement of the liquid–gas ratio increases the effective contact area between the CS_2 gas and the NMP liquid, thereby improving the mass transfer efficiency of the liquid–gas interface. However, when the liquid–gas ratio is increased to a certain level, the effective contact area is already large enough. The effect of further improving the liquid–gas ratio on the mass removal efficiency is not obvious, while the energy consumption continues to increase.

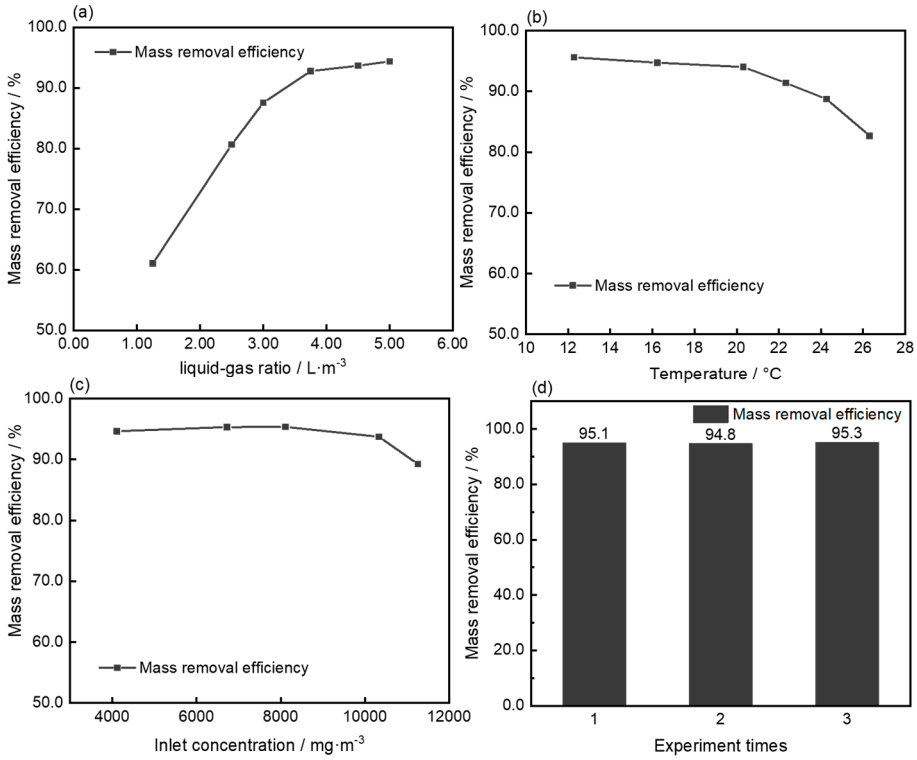

Figure 4. Absorption process research: (**a**) The effect of liquid-gas ratio on absorption, (**b**) The effect of temperature on absorption, (**c**) The effect of inlet concentration on absorption, (**d**) Repeated absorption experiments.

It can be seen from Figure 4b that increasing the temperature will lead to a decrease in the mass removal efficiency, and the decrease in the mass removal efficiency is particularly significant when the temperature exceeds 20 °C. The main reason for this phenomenon is that the increase of temperature will increase the kinetic energy of each molecule in the absorbent, and it will both weaken the interaction between CS_2 and NMP molecules and increase the desorption rate, resulting in a decrease in the absorption of CS_2 molecules by NMP.

Figure 4c shows the experimental results of the absorption of CS_2 waste air with six different intake concentrations. It can be seen from Figure 4c that the mass removal efficiency of NMP to CS_2 first increases and then decreases sharply with the increase of the concentration. According to double film theory, the increasing intake air concentration of CS_2 will increase the CS_2 partial pressure in the gas film and enhance the driving force of the mass transfer process, promoting the CS_2 waste air absorption process. However, when the intake air concentration of CS_2 is more significant than 10,000 mg·m^{-3}, the dissolution capacity of the absorbent for CS_2 is limited by the solubility, i.e., the absorber reaches saturation, resulting in a sharp decline in the mass removal efficiency. Meanwhile, the similar conclusion was reached by Qing et al. [42] when they studied the effect of CO_2 inlet concentration on the CO_2 removal rate.

Figure 4d shows the results of three groups of absorption experiments carried out under the above process conditions, and the average mass removal efficiency is up to 95.2%. To sum up, the optimal process conditions for NMP to absorb CS_2 waste air are the liquid–gas ratio of 3.75 L·m^{-3}, a temperature of 20 °C, and an intake air concentration lower than 10,000 mg·m^{-3}.

3.3. Analysis of Desorption Experiment Results

3.3.1. Regeneration of Lean Liquid Resorption Performance

Figure 5a,b show the effects of water content and CS_2 content in NMP on the mass removal efficiency, respectively. Figure 5c shows the results of the synergistic effect of water content and CS_2 content in NMP on the mass removal efficiency. In Figure 5a,b, the mass removal efficiency decreased sharply with the increase of water content and CS_2 content in NMP. When the moisture content exceeds 1.00%, or the CS_2 content exceeds 0.5‰, the mass removal efficiency will drop to less than 90.0%.

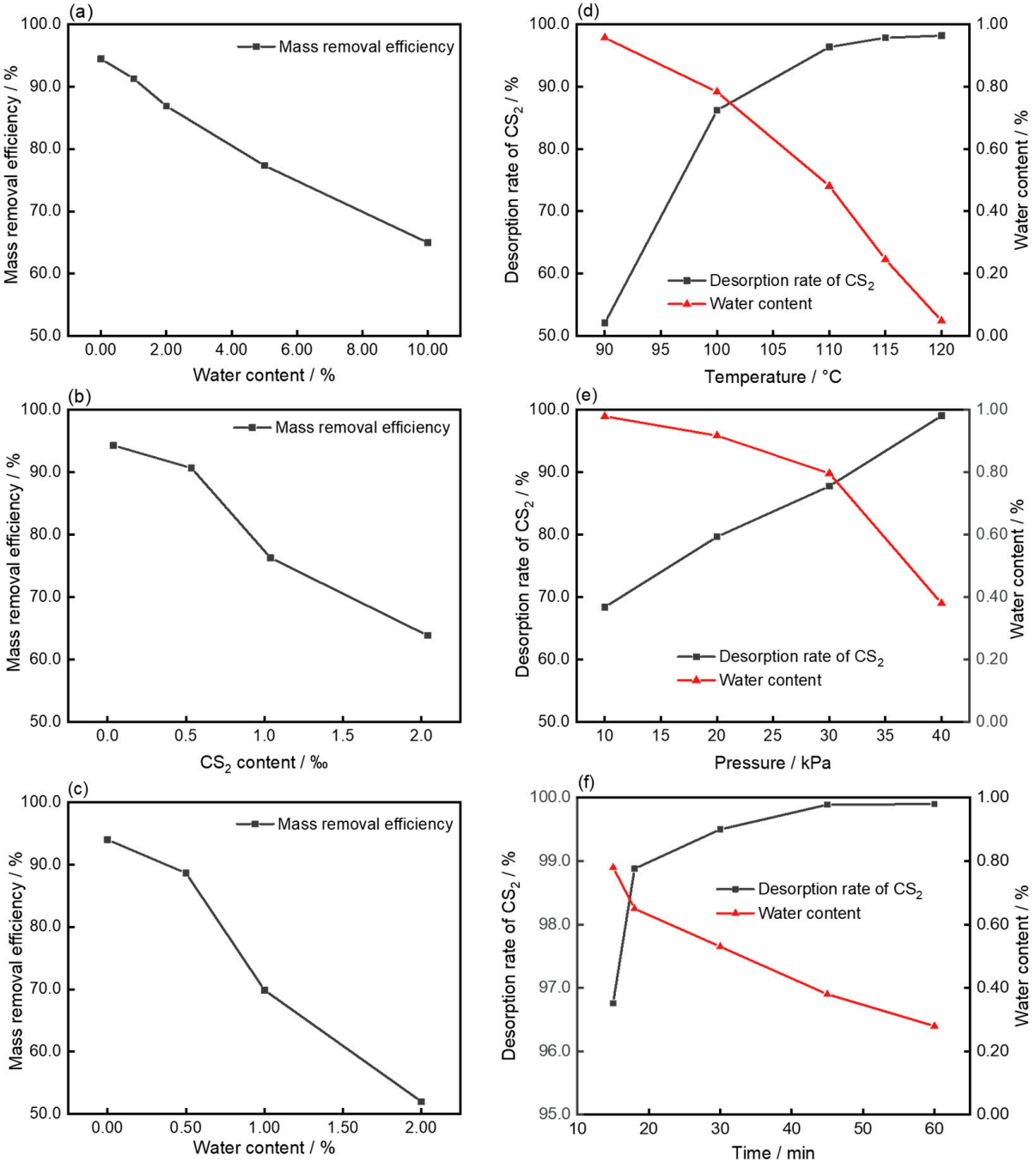

Figure 5. Desorption process research: (**a**) The effect of water content on absorption (CS_2-free), (**b**) The effect of CS_2 content on absorption (water-free), (**c**) The effect of water and CS_2 content on absorption (0.5‰ CS_2), (**d**) The effect of temperature on desorption, (**e**) The effect of pressure on desorption, (**f**) The effect of time on desorption.

In Figure 5c, the CS_2 content in the fixed NMP was kept constant at 0.5%. The water content was controlled within 0.5%, and the mass removal efficiency can be maintained above 89.0%. Therefore, to ensure that the desorbed absorbent retains excellent absorption, the CS_2 content in the regenerated absorbent must be controlled within 0.5% and the water content within 0.50%. Comparing Figure 5b,c, it can be seen that NMP containing CS_2 and water at the same time will make the mass removal efficiency drop more obviously, that is, the effect of the two on the mass removal efficiency has a synergistic effect. The effect of water content on CS_2 uptake by NMP is similar to the findings of Fu et al. [43] on the effect of water content on CO_2 uptake.

3.3.2. Desorption Process Conditions

Figure 5d,e show the effects of temperature and pressure on the desorption effect, respectively. When the constant pressure is 10 kPa, the CS_2 desorption rate increases with the increase of temperature. When the temperature reaches 115 °C, the desorption rate is close to 99.0%. At this time, the CS_2 desorption is relatively complete. The water is continuously vaporized, and the water content in the rich liquid is continuously reduced. At a constant temperature of 115 °C, the lower the pressure, the better the desorption of the rich liquid, the higher the CS_2 desorption rate, and the lower the water content in the rich liquid. When the pressure is 10 kPa, the CS_2 desorption rate is 99.1%, and the water content is 0.55%. At this time, the regeneration lean liquid has good absorption performance after desorption. Figure 5f shows the effect of desorption time on the desorption effect. When the desorption time was 45 min, the CS_2 desorption rate reached 99.9%, and the water content in the regenerated lean liquid after desorption was 0.38%. At this time, the desorbed absorbent had good absorption performance, and the mass removal efficiency could be maintained above 90%.

Altogether, the optimal desorption process conditions for absorbing rich liquid are: temperature 115 °C, pressure 10 kPa, and desorption time 45 min. Figure 6a shows three groups of desorption experiments carried out under the abovementioned process conditions; the average desorption rate reaches 99.6%, and the average water content after desorption is 0.39%.

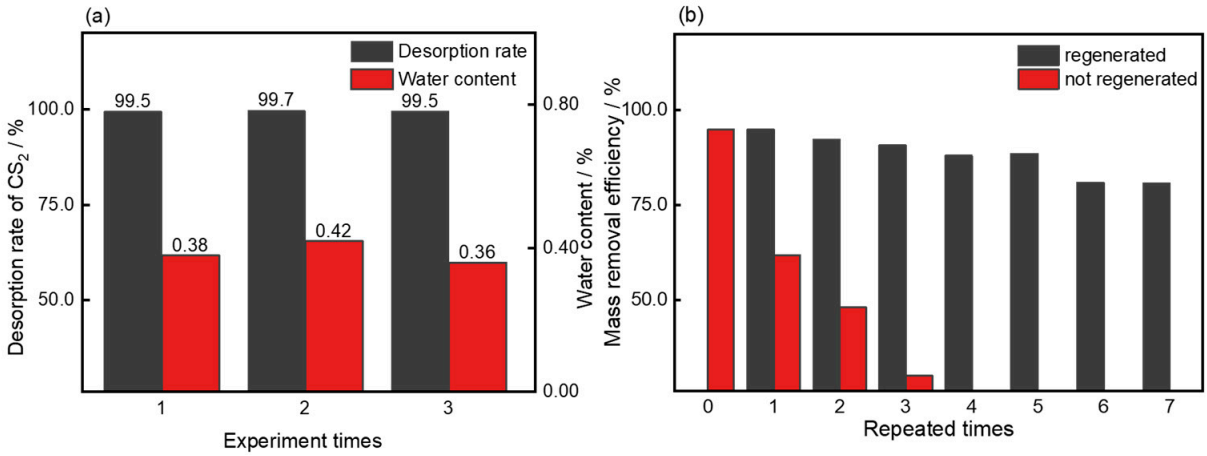

Figure 6. Absorbent regeneration experiment: (**a**) Repeated desorption experiments, (**b**) Regenerated lean liquid circulation absorption experiment.

3.3.3. NMP Absorbent Cyclic Absorption Performance

Figure 6b shows the experimental results of multiple absorptions of CS_2 exhaust gas with the regenerated and unregenerated absorber. As shown in Figure 6b, when the NMP-rich liquid without desorption is subjected to the cyclic absorption experiment, it no longer has the absorption capacity after four absorption operations. However, the mass removal efficiency of the desorbed NMP lean liquid can reach more than 90.0% in

the first three times, and the mass removal efficiency of the regenerated lean liquid after seven times of desorption can still be maintained at 80.6%. Due to incomplete regeneration and continuous loss of absorbent during regeneration, the mass removal efficiency of the regeneration lean liquid shows a trend of gradual deterioration. In engineering, the mass removal efficiency of regeneration lean liquid can be restored by intermittently replenishing fresh NMP solvent.

4. Conclusions

In this paper, the theory of the maximum excess Gibbs function and the absorption potential for screening absorbents were successfully introduced to the process of CS_2 waste air absorbent screening. Based on the absorption experiments, we concluded that it is feasible in low-viscosity systems. At the same time, NMP with slight toxicity and easy regeneration was selected as a highly efficient absorbent to recycle CS_2 (95.2%). Our method of screening absorbents is simpler and more efficient than previous methods of evaluating absorbents and has a broader range of applications [34–36]. Moreover, the optimal process conditions for NMP to absorb CS_2 waste air are: liquid–gas ratio 3.75 $L \cdot m^{-3}$, temperature 20 °C, and intake air concentration lower than 10,000 $mg \cdot m^{-3}$. The regenerated lean liquid has excellent resorption performance and can be recycled.

In summary, we simplify the screening steps of CS_2 waste air absorbent in a low-viscosity system, contributing to efficiently screening absorbents with low operating cost. Meanwhile, we believe that further design of low-cost composite absorbers should also prioritize NMP as the primary component. This paper has significant application value for recycling CS_2 waste air in viscose fiber plants and reducing CS_2 pollution and carbon emissions from the source.

Author Contributions: Conceptualization, M.C., X.Z. and B.F.; methodology, J.L.; software, K.C. and R.X.; validation, J.L., K.C. and M.C.; investigation, R.X.; data curation, K.C.; writing—original draft preparation, R.X.; writing—review and editing, R.X.; funding acquisition, M.C., X.Z. and B.F. All authors have read and agreed to the published version of the manuscript.

Funding: The project is supported financially by the National Natural Science Foundation of China (No. 21606133), and the Jiangsu Province Industry University Research Prospective Joint Research Project (BY2016006-02).

Institutional Review Board Statement: Not applicable.

Informed Consent Statement: Not applicable.

Data Availability Statement: The data will be available upon reasonable request.

Conflicts of Interest: The authors declare no competing financial interest.

References

1. Aldalbahi, A.; El-Naggar, M.E.; El-Newehy, M.H.; Rahaman, M.; Hatshan, M.R.; Khattab, T.A. Effects of Technical Textiles and Synthetic Nanofibers on Environmental Pollution. *Polymers* **2021**, *13*, 155. [CrossRef] [PubMed]
2. Smet, E.; Lens, P.; Langenhove, H.V. Treatment of Waste Gases Contaminated with Odorous Sulfur Compounds. *Crit. Rev. Environ. Sci. Technol.* **2010**, *28*, 89–117. [CrossRef]
3. Anwar, K.; Benjamin, R.; Simon, G.; Carl, P.; Dudley, S. Global analysis of carbon disulfide (CS_2) using the 3-D chemistry transport model STOCHEM. *AIMS Environ. Sci.* **2017**, *4*, 484–501. [CrossRef]
4. Chin, M.; Davis, D. Global sources and sinks of OCS and CS_2 and their distributions. *Global Biogeochem. Cycles* **1993**, *7*, 321–337. [CrossRef]
5. Lee, C.-L.; Brimblecombe, P. Anthropogenic contributions to global carbonyl sulfide, carbon disulfide and organosulfides fluxes. *Earth-Sci. Rev.* **2016**, *160*, 1–18. [CrossRef]
6. Zeng, Z.; Altarawneh, M.; Dlugogorski, B.Z. Atmospheric oxidation of carbon disulfide (CS_2). *Chem. Phys. Lett.* **2017**, *669*, 43–48. [CrossRef]
7. Zhu, C.; Lu, J.; Wang, X.; Huang, Q.; Huang, L.; Wang, J. Removal of Carbon Disulfide from Gas Streams Using Dielectric Barrier Discharge Plasma Coupled with MnO_2 Catalysis System. *Plasma Chem. Plasma Process.* **2013**, *33*, 569–579. [CrossRef]
8. Wu, Y.; Wang, Z. Research progress in reproductive toxicity of carbon disulfide among exposed workers. *Chin. J. Public Health* **2016**, *32*, 1133–1136.

9. Chalansonnet, M.; Carreres-Pons, M.; Venet, T.; Thomas, A.; Merlen, L.; Boucard, S.; Cosnier, F.; Nunge, H.; Bonfanti, E.; Llorens, J.; et al. Effects of co-exposure to CS_2 and noise on hearing and balance in rats: Continuous versus intermittent CS_2 exposures. *J. Occup. Med. Toxicol.* **2020**, *15*, 9. [CrossRef]
10. Venet, T.; Carreres-Pons, M.; Chalansonnet, M.; Thomas, A.; Merlen, L.; Nunge, H.; Bonfanti, E.; Cosnier, F.; Llorens, J.; Campo, P. Continuous exposure to low-frequency noise and carbon disulfide: Combined effects on hearing. *Neurotoxicology* **2017**, *62*, 151–161. [CrossRef]
11. Schramm, A.; Uter, W.; Brandt, M.; Goen, T.; Kohrmann, M.; Baumeister, T.; Drexler, H. Increased intima-media thickness in rayon workers after long-term exposure to carbon disulfide. *Int. Arch. Occup. Environ. Health* **2016**, *89*, 513–519. [CrossRef]
12. Li, K.; Ning, P.; Li, K.; Wang, C.; Sun, X.; Tang, L.; Liu, S. Low Temperature Catalytic Hydrolysis of Carbon Disulfide on Activated Carbon Fibers Modified by Non-thermal Plasma. *Plasma Chem. Plasma Process.* **2017**, *37*, 1175–1191. [CrossRef]
13. Song, X.; Chen, X.; Sun, L.; Li, K.; Sun, X.; Wang, C.; Ning, P. Synergistic effect of Fe_2O_3 and CuO on simultaneous catalytic hydrolysis of COS and CS_2: Experimental and theoretical studies. *Chem. Eng. J.* **2020**, *399*, 125764. [CrossRef]
14. Song, X.; Ning, P.; Wang, C.; Li, K.; Tang, L.; Sun, X.; Ruan, H. Research on the low temperature catalytic hydrolysis of COS and CS_2 over walnut shell biochar modified by Fe–Cu mixed metal oxides and basic functional groups. *Chem. Eng. J.* **2017**, *314*, 418–433. [CrossRef]
15. Li, Q.; Yi, H.; Tang, X.; Zhao, S.; Zhao, B.; Liu, D.; Gao, F. Preparation and characterization of Cu/Ni/Fe hydrotalcite-derived compounds as catalysts for the hydrolysis of carbon disulfide. *Chem. Eng. J.* **2016**, *284*, 103–111. [CrossRef]
16. Glarborg, P.; Halaburt, B.; Marshall, P.; Guillory, A.; Troe, J.; Thellefsen, M.; Christensen, K. Oxidation of reduced sulfur species: Carbon disulfide. *J Phys Chem A* **2014**, *118*, 6798–6809. [CrossRef]
17. Chen, J.; Chen, A.; Qiu, P.; Huang, L.; Zhou, Q. Removal of carbon disulfide from air stream by absorption combined with electrochemical oxidation. *J. Environ. Chem. Eng.* **2019**, *7*, 103167. [CrossRef]
18. Xia, G.; Zhou, X.; Hu, J.; Sun, Z.; Yao, J.; Chen, D.; Wang, J. Simultaneous removal of carbon disulfide and hydrogen sulfide from viscose fibre waste gas with a biotrickling filter in pilot scale. *J. Clean. Prod.* **2019**, *230*, 21–28. [CrossRef]
19. Prenafeta-Boldu, F.X.; Rojo, N.; Gallastegui, G.; Guivernau, M.; Vinas, M.; Elias, A. Role of Thiobacillus thioparus in the biodegradation of carbon disulfide in a biofilter packed with a recycled organic pelletized material. *Biodegradation* **2014**, *25*, 557–568. [CrossRef]
20. Rojo, N.; Gallastegi, G.; Barona, A.; Gurtubay, L.; Ibarra-Berastegi, G.; Elías, A. Biotechnology as an alternative for carbon disulfide treatment in air pollution control. *Environ. Rev.* **2010**, *18*, 321–332. [CrossRef]
21. Samanta, A.; Zhao, A.; Shimizu, G.K.H.; Sarkar, P.; Gupta, R. Post-Combustion CO_2 Capture Using Solid Sorbents: A Review. *Ind. Eng. Chem. Res.* **2012**, *51*, 1438–1463. [CrossRef]
22. Gunawardene, O.H.P.; Gunathilake, C.A.; Vikrant, K.; Amaraweera, S.M. Carbon Dioxide Capture through Physical and Chemical Adsorption Using Porous Carbon Materials: A Review. *Atmosphere* **2022**, *13*, 397. [CrossRef]
23. Zhang, X.-F.; Wang, Z.; Ding, M.; Feng, Y.; Yao, J. Advances in cellulose-metal organic framework composites: Preparation and applications. *J. Mater. Chem. A* **2021**, *9*, 23353–23363. [CrossRef]
24. Gunathilake, C.A.; Ranathunge, G.G.T.A.; Dassanayake, R.S.; Illesinghe, S.D.; Manchanda, A.S.; Kalpage, C.S.; Rajapakse, R.M.G.; Karunaratne, D.G.G.P. Emerging investigator series: Synthesis of magnesium oxide nanoparticles fabricated on a graphene oxide nanocomposite for CO_2 sequestration at elevated temperatures. *Environ. Sci. Nano* **2020**, *7*, 1225–1239. [CrossRef]
25. Gunathilake, C.A.; Dassanayake, R.S.; Fernando, C.A.N.; Jaroniec, M. Zirconium Containing Periodic Mesoporous Organosilica: The Effect of Zr on CO_2 Sorption at Ambient Conditions. *J. Compos. Sci.* **2022**, *6*, 168. [CrossRef]
26. McGuirk, C.M.; Siegelman, R.L.; Drisdell, W.S.; Runcevski, T.; Milner, P.J.; Oktawiec, J.; Wan, L.F.; Su, G.M.; Jiang, H.Z.H.; Reed, D.A.; et al. Cooperative adsorption of carbon disulfide in diamine-appended metal-organic frameworks. *Nat. Commun.* **2018**, *9*, 5133. [CrossRef]
27. Jin, J.; Zhang, Z.; Bai, H. Preparation and performance of γ-Fe_2O_3/AC desulfurizer at low temperature for CS_2 removal. *Chem. Ind. Eng. Prog.* **2018**, *37*, 4397–4404. [CrossRef]
28. Nagarajan, V.; Chandiramouli, R. CS_2 And H_2S adsorption studies on novel hex-star phosphorene nanosheet—A DFT perspective. *Mol. Phys.* **2022**, *120*, 2066027. [CrossRef]
29. Heldebrant, D.J.; Yonker, C.R.; Jessop, P.G.; Phan, L. Reversible uptake of COS, CS_2, and SO_2: Ionic liquids with O-alkylxanthate, O-alkylthiocarbonyl, and O-alkylsulfite anions. *Chemistry* **2009**, *15*, 7619–7627. [CrossRef]
30. Huo, Z.; Shen, B.; Chen, X.; Sun, H.; Zhan, G.; Yu, H. Compositional design of UDS and its application on removal of CS_2 from viscose fiber waste gas. *Chem. Ind. Eng. Prog.* **2018**, *37*, 292–300. [CrossRef]
31. Bai, Y.; Yu, M.; Zhang, X.-F.; Yao, J. Deep eutectic solvent assisted preparation of ZnO deposited carbonized wood for efficient CO_2 storage and oil absorption. *J. Mol. Liq.* **2023**, *376*, 121409. [CrossRef]
32. Zhu, X.; Fan, Z.; Zhang, X.-F.; Yao, J. Metal-organic frameworks decorated wood aerogels for efficient particulate matter removal. *J. Colloid Interface Sci.* **2023**, *629*, 182–188. [CrossRef]
33. Wang, D.; Xie, J.; Zhou, H.; Liu, L.; Li, H.; Li, G.; Fan, X. Multiscale energy reduction of amine-based absorbent SO2 capture technology: Absorbent screening and process improvement. *Sep. Purif. Technol.* **2022**, *301*, 121949. [CrossRef]
34. Lhuissier, M.; Couvert, A.; Kane, A.; Amrane, A.; Audic, J.-L.; Biard, P.-F. Volatile organic compounds absorption in a structured packing fed with waste oils: Experimental and modeling assessments. *Chem. Eng. Sci.* **2021**, *238*, 116598. [CrossRef]

35. Rodriguez Castillo, A.-S.; Biard, P.-F.; Guihéneuf, S.; Paquin, L.; Amrane, A.; Couvert, A. Assessment of VOC absorption in hydrophobic ionic liquids: Measurement of partition and diffusion coefficients and simulation of a packed column. *Chem. Eng. J.* **2019**, *360*, 1416–1426. [CrossRef]
36. Wang, B.; Zhang, X.; Shang, D.; Fen, J.; Wu, H.; Zhang, Y.; Li, J. Efficient Recovery of Dichloromethane by [Bmim][PF6] and Process Simulation. *Chin. J. Process Eng.* **2018**, *18*, 82–87. [CrossRef]
37. Wang, C.; Zhang, Y.; Han, J.; Zhang, M. Analysis of influencing factors for determination of carbon disulfide in ambient air by diethylamine spectrophotometry. *Instrum. Anal. Monit.* **2009**, *97*, 44–46. [CrossRef]
38. Wang, Y.-n.; Xu, R.; Kai, Y.; Wang, H.; Sun, Y.; Zhan, M.; Gong, B. Evaluating the physicochemical properties of refuse with a short-term landfill age and odorous pollutants emission during landfill mining: A case study. *Waste Manag.* **2021**, *121*, 77–86. [CrossRef] [PubMed]
39. Ma, H.; Wang, Z.; Zhang, X.-F.; Ding, M.; Yao, J. In situ growth of amino-functionalized ZIF-8 on bacterial cellulose foams for enhanced CO_2 adsorption. *Carbohydr. Polym.* **2021**, *270*, 118376. [CrossRef] [PubMed]
40. Gunathilake, C.; Dassanayake, R.S.; Kalpage, C.S.; Jaroniec, M. Development of Alumina–Mesoporous Organosilica Hybrid Materials for Carbon Dioxide Adsorption at 25 C. *Materials* **2018**, *11*, 2301. [CrossRef]
41. Song, D.; Seibert, A.F.; Rochelle, G.T. Mass Transfer Parameters for Packings: Effect of Viscosity. *Ind. Eng. Chem. Res.* **2018**, *57*, 718–729. [CrossRef]
42. Qing, Z.; Yincheng, G.; Zhenqi, N. Experimental studies on removal capacity of carbon dioxide by a packed reactor and a spray column using aqueous ammonia. *Energy Procedia* **2011**, *4*, 519–524. [CrossRef]
43. Fu, K.; Zheng, M.; Wang, H.; Fu, D. Effect of water content on the characteristics of CO_2 capture processes in absorbents of 2-ethylhexan-1-amine + diglyme. *Energy* **2022**, *244*, 122656. [CrossRef]